EPJ manuscript No.
(will be inserted by the editor)

Forward and midrapidity charmonium production at RHIC

Xingbo Zhao[1] and Ralf Rapp[1]

Cyclotron Institute and Physics Department, Texas A&M University, College Station, TX 77843-3366, USA

Received: date / Revised version: date

Abstract. J/ψ production at forward and midrapidity at the Relativistic Heavy-Ion Collider (RHIC) is calculated within a previously constructed rate-equation approach accounting for both direct production and regeneration from c and $\bar{c}$. The results are compared to experimental data. The observed stronger suppression at forward rapidity can be qualitatively explained by a smaller statistical regeneration component together with stronger cold nuclear matter induced suppression compared to midrapidity. The χ_c over J/ψ ratio and ψ' over J/ψ ratio are also calculated.

PACS. 12.38.Mh Quark-Gluon Plasma – 25.75.-q Relativistic Heavy-Ion Collisions – 14.40.Lb Charmed Mesons

1 Introduction

The suppression of J/ψ mesons in ultrarelativistic heavy-ion collisions, as a result of color Debye screening, has been suggested as a signature [1] of Quark-Gluon Plasma (QGP) formation a long time ago and is indeed observed in both *Pb-Pb* collisions at the CERN Super Proton Synchrotron (SPS) [2] and in *Au-Au* collisions at BNL Relativistic Heavy-Ion Collider (RHIC) [3]. However, it is puzzling that the observed suppression is very comparable at SPS and RHIC energies, since the energy density of the medium at RHIC is expected to be much higher than at SPS. The statistical model [4], or kinetic approaches [5, 6], explain this puzzle by considering the regeneration of charmonium from c and $\bar{c}$ quarks: at RHIC energies more c and $\bar{c}$ quarks (relative to charmonium) are produced than at SPS energies and therefore the regeneration of charmonium at RHIC largely compensates the expected stronger suppression (which was, in fact, predicted in Ref. [7]). Recent RHIC data [3] suggest another puzzle: charmonium suppression observed at forward rapidity ($|y| \in [1.2,2.2]$) is stronger than at midrapidity ($|y| < 0.35$), despite the energy density of the medium at forward rapidity being presumably smaller which should lead to weaker suppression.

J/ψ production at forward rapidity has been investigated by several theoretical models. In the kinetic recombination model [8] the rapidity and transverse momentum distributions of J/ψ are obtained through solving a rate equation with the gain term accounting for the continuous formation process of the J/ψ's from c and $\bar{c}$ quarks throughout the QGP. The "input" charm-quark spectra are obtained from either perturbative QCD (pQCD) calculations or thermal distributions and the inelastic reaction employed is the traditional gluo-dissociation process [9]. A narrowing of the J/ψ rapidity distribution is predicted in *A-A* relative to *p-p* collisions. In the statistical hadronization model (SHM) [10] all charmonia are produced from coalescence of c and $\bar{c}$ quarks at the hadronization transition. The relative abundance of open and hidden charm states is determined by their mass and spin-isospin degeneracy, based on the assumption of thermal equilibrium at the hadronization temperature, T_c. The resulting J/ψ rapidity distributions from the SHM are also narrower in *A-A* than in *p-p* collisions, but significantly wider than those from the kinetic recombination approach, mostly due to broader input distributions of charm-quark cross section. In the comovers interaction model (CIM) [11] the primordially produced J/ψ's are subject to a series of cold nuclear matter induced (initial state) effects and subsequently destroyed by "comovers" in the medium with an effective dissociation cross section; $\sigma_{Diss} \sim$0.65-1 mb. The CIM has recently been augmented by including charm quark coalescence into J/ψ [12]. The rapidity dependence of experimental data is reproduced both for *Au-Au* and *Cu-Cu* collisions at RHIC, mostly due to initial-state effects in the incoming nuclei.

In the present work we apply a rate-equation approach [5,6] to 200 AGeV *Au-Au* collisions at RHIC, to calculate J/ψ production at forward rapidity and compare to previously obtained midrapidity results [6]. The approach assumes a thermalized medium (QGP and subsequent hadronic gas (HG)) in which anomalous suppression and regeneration from coalescence of c-$\bar{c}$ quarks and D-$\bar{D}$ mesons occur. In Section 2 we evaluate cold nuclear matter effects which affect the charmonium abundances before the medium thermalizes. We then recall basic ingredients of our approach to evaluate J/ψ suppression and regeneration in QGP and HG phase in Section 3. We discuss the numerical results for the centrality dependence of the in-

clusive J/ψ yield and $\langle p_t^2\rangle$ as well as χ_c to J/ψ and ψ' to J/ψ ratios in Section 4 and the J/ψ transverse momentum spectra in Section 5. Conclusions are given in Section 6.

2 Cold nuclear matter effects

A "pre-charmonium" $c\bar{c}$ pair produced in an initial hard nucleon-nucleon (N-N) collision first travels through the incident (cold) nuclei before becoming a fully formed charmonium ($\Psi = J/\psi, \chi_c, \psi'$). The modification of initial parton distribution functions, affecting the hard production of pre-charmonium, and the interactions between pre-Ψ and cold nuclei are referred to as cold nuclear matter (CNM) effects. The latter provide a baseline for identifying the anomalous suppression and/or enhancement of charmonia which is hoped to give insights about the subsequent hot medium. An accurate estimate of CNM effects is therefore mandatory. In the present work we assume CNM effects to be the only relevant ones to charmonium production before the medium thermalizes and investigate them within the following two schematic baseline scenarios: (1) Nuclear absorption + Cronin effect. (2) Shadowing + Nuclear absorption + Cronin effect.

Let us start with scenario 1: The initial dissociation by primordial nucleons passing by is described by the standard Glauber model resulting in a spatial charmonium distribution at the thermalization time τ_0,

$$f_\Psi(\boldsymbol{x}_t,\tau_0) = \sigma_{pp}^\Psi \int d^2s\; dz\; dz' \rho_A(\boldsymbol{s},z)\; \rho_B(\boldsymbol{x}_t-\boldsymbol{s},z') \times \exp\left\{-\int_z^\infty dz_A \rho_A(\boldsymbol{s},z_A)\sigma_{nuc}\right\} \times \exp\left\{-\int_{z'}^\infty dz_B \rho_B(\boldsymbol{x}_t-\boldsymbol{s},z_B)\sigma_{nuc}\right\}\;, \quad (1)$$

where $\rho_{A,B}$ are Woods-Saxon profiles [13] of nuclei A and B. The nuclear absorption cross section, σ_{nuc}=1.5 mb (σ_{nuc}=2.7 mb for ψ'), serves as a parameter to regulate the strength of dissociation due to all CNM effects combined, estimated from midrapidity d-Au collisions [14]. Shadowing effects are effectively parameterized into σ_{nuc}, which we furthermore assume to be rapidity-independent. Such a scenario may be justified if shadowing in one Au nucleus (forward rapidity in d-Au) is roughly compensated by anti-shadowing in the other Au nucleus (backward rapidity in d-Au). In addition to absorption, transverse momentum (p_t) spectra of (pre)Ψ's are broadened compared to p_t spectra in p-p collisions due to the Cronin effect. We assume the physical mechanism of the Cronin effect to be the rescattering of gluons in the CNM before they fuse into charmonium. Therefore, the increase of $\langle p_t^2\rangle$ is proportional to the mean length, $\langle l\rangle$, the gluon travels in CNM assuming a random walk treatment of the gluon rescattering, resulting in $\Delta\langle p_t^2\rangle = \langle p_t^2\rangle_{AA} - \langle p_t^2\rangle_{pp} = a_{gN}\langle l\rangle$. The proportionality coefficient a_{gN} can in principle be estimated from d-Au data: here we adopt a_{gN}=0.1 GeV^2/fm which is compatible with SPS NA50 data [15] and current RHIC data [14]. At forward rapidity the d-Au data show a p_t broadening of $\Delta\langle p_t^2\rangle$=$\langle p_t^2\rangle_{dAu}$ − $\langle p_t^2\rangle_{pp}$=0.8±0.4 GeV^2 [14] (we combined the uncertainty for $\langle p_t^2\rangle$ of d-Au and p-p in quadrature). With a "path length" $\langle l\rangle$=4 fm for d-Au collisions [15] we estimate an uncertainty of a_{gN}=0.1∼0.3 GeV^2/fm in our numerical calculations and then we perform a Gaussian smearing over the input power-law p_t spectra from p-p data with $\Delta\langle p_t^2\rangle$=$a_{gN}\langle l\rangle$.

Concerning scenario 2 we follow the treatment of Ref. [12] and separately treat nuclear absorption, shadowing and Cronin effect. The total suppression by CNM effects (nuclear absorption + shadowing) in this scenario is comparable to the scenario 1 at midrapidity but is stronger at forward rapidity due to stronger shadowing at forward rapidity. Concerning p_t distributions and Cronin effect our treatment in this scenario is identical to scenario 1.

3 Kinetic charmonium production approach

We assume that the medium formed at RHIC reaches thermal equilibrium at about τ_0=1/3 fm/c and use a thermal rate equation thereafter to describe the subsequent evolution of Ψ's according to,

$$\frac{\mathrm{d}N_\Psi}{\mathrm{d}\tau} = -\Gamma_\Psi\; (N_\Psi - N_\Psi^{\mathrm{eq}})\;, \quad (2)$$

(as usual, we account the feeddown from χ_c's and ψ''s to J/ψ's; formation time effects, as considered in Ref. [16], are not included in the present analysis). The initial condition follows from CNM effects discussed in the previous section. The loss term, $-\Gamma_\Psi N_\Psi$, accounts for the dissociation of the primordially produced charmonium and the gain term, $\Gamma_\Psi N_\Psi^{\mathrm{eq}}$, for the regeneration of charmonia via coalescence of c and $\bar{c}$ quarks. Γ_Ψ is the in-medium charmonia dissociation rate and N_Ψ^{eq} is the equilibrium limit of the charmonium abundances. The rate equation treats the coalescence of c and $\bar{c}$ quarks as a continuous process over the course of medium evolution in line with lattice QCD [17] and potential-model results [18] which suggest the J/ψ to survive at temperatures well above the critical temperature T_c.

Let us first address the dissociation of primordially produced charmonia (direct component), which is identified as the solution of the homogeneous rate equation with only the loss term included. In our previously constructed kinetic approach a Boltzmann transport equation is employed to describe the evolution of the charmonium phase space distribution functions $f_\Psi(\boldsymbol{x},\boldsymbol{p},\tau)$ in a thermalized medium with initial distribution from Eq. (1),

$$p^\mu \partial_\mu f_\Psi(\boldsymbol{x},\boldsymbol{p},\tau) = -E_\Psi\; \Gamma_\Psi(\boldsymbol{x},\boldsymbol{p},\tau)\; f_\Psi(\boldsymbol{x},\boldsymbol{p},\tau)\;. \quad (3)$$

We neglect elastic charmonium rescattering and only account for parton(hadron)-induced inelastic scattering. The momentum-dependent dissociation rate Γ_Ψ is calculated via a convolution of the charmonium dissociation cross section, σ^{diss}, with a thermal distribution $f(\omega;T)$ of particles from the heat bath (QGP or HG) and their relative

velocity v_{rel}, with charmonia [6],

$$\Gamma_\Psi(\boldsymbol{x},\ \boldsymbol{p},\ \tau) = \sum_i \int \frac{d^3k}{(2\pi)^3}\ f^i(\omega_k;T(\tau))\ \sigma_{\Psi i}^{diss}\ v_{rel}\ . \quad (4)$$

In QGP we include the in-medium reduction of charmonium binding energy due to color Debye screening. Under these circumstances the gluo-dissociation process $\Psi + g \to c + \bar{c}$ [9] is ineffective to destroy a charmonium [7] and we instead employ a quasifree dissociation process: $i + \Psi \to i + c + \bar{c}$ (i=g,q,$\bar{q}$) [7]. The strong coupling constant α_s in the quasifree cross section is one of the two main parameters in our approach and is adjusted to reproduce the J/ψ yield in central Pb-Pb collisions at SPS (resulting in α_s=0.24, cf. the upper panel of Fig. 2). The comparison between the charmonium 3-momentum dependence of gluo-dissociation (with vacuum binding energy) and quasifree rates (with in-medium binding energy) can be found in Ref. [6]: these two dissociation rates are comparable for low-momentum J/ψ but at high momentum the gluo-dissociation rate is significantly smaller than the quasifree one; for χ_c the gluo-dissociation rate is much larger than quasifree rate. It is noteworthy that the so-called "leakage effect" [19,20,21] is accounted for by the Boltzmann transport equation approach: high p_t charmonia which travel outside the fireball are not subject to suppression anymore rendering less suppression.

To solve the transport equation (3) we need to know the medium temperature evolution, $T(\tau)$, which is determined in the following way: We assume the total entropy to be produced at the thermalization time (τ_0=1/3 fm/c at RHIC). The subsequent expansion is approximated by a cylindrically and isentropically expanding fireball,

$$V_{FB}(\tau) = (z_0 + v_z\tau)\ \pi\ (r_0 + \frac{1}{2}a_\perp\tau^2)^2\ . \quad (5)$$

A freeze-out temperature of $T_{fo} \simeq 120$ MeV terminates the evolution and results in $\tau_{fo} = 10-15$ fm/c. The fireball covers 1.8 rapidity units and the initial transverse radius r_0 represents the initial transverse overlap of the two colliding Au nuclei at a given impact parameter b. The expansion parameters $v_z, a_z, a_\perp$ capture the main aspects of hydrodynamic calculations to reproduce observed flow velocities. For simplicity we assume that the expansion parameters are the same for midrapidity ($|y|$ <0.35) and forward rapidity ($|y| \in$[1.2,2.2]). The total entropy is, however, different, being inferred from number of the charged-particle rapidity density, for which we use BRAHMS data [22] dN_{ch}/dy=660 at midrapidity and dN_{ch}/dy=615 at forward rapidity (for 0-5% centrality); PHOBOS [23] and PHENIX [24] give consistent results with slightly larger charged particle multiplicities at both midrapidity and forward rapidity. For the equation of state (EoS) we use an ideal gas of massive quarks and gluons for $T > T_c$ and a resonance gas equation of state for $T < T_c$ including the 37 lowest lying mesons and 37 lowest lying baryons. The critical temperature, T_c=180 MeV, at RHIC 200 AGeV is in line with thermal-model fits of particle ratios and the current predictions of lattice QCD [25]. Combining entropy conservation and EoS the temperature evolution profile follows as a function of time τ as displayed in Fig. 1 for central Au-Au collisions at both midrapidity and forward rapidity, and compared to SPS Pb-Pb $\sqrt{s}$=17.3 AGeV collisions. We can see that the lifetime of QGP at forward rapidity is a slightly shorter than at midrapidity due to less produced particles and smaller energy densities.

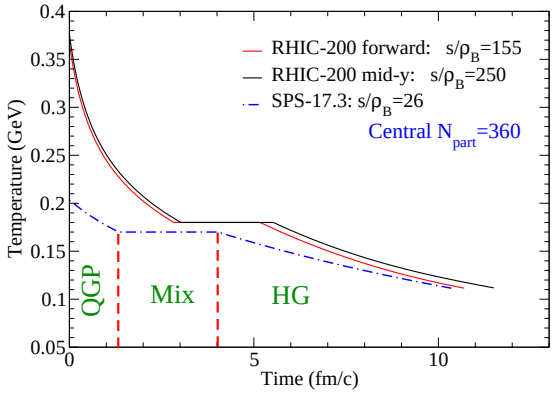

Fig. 1. (Color online) Temperature profiles at RHIC 200 AGeV (solid line: midrapidity; dashed line: forward rapidity) and at SPS 17.3 AGeV (dot-dashed line) for central collisions (N_{part}=360) of heavy nuclei.

Now we turn to the regeneration component which is identified as the difference between the solution of the full rate equation (2) and the equation without the gain term, $\Gamma_\Psi N_\Psi^{\rm eq}$ on r.h.s. The latter is dictated by detailed balance with Γ_Ψ the same (dissociation) rate for the direct component. For the charmonium abundances in equilibrium limit, $N_\Psi^{\rm eq}$, we employ the statistical model [10] with $N_\Psi^{\rm eq}$=$N_\Psi^{\rm stat}\mathcal{R}$, where $\mathcal{R}$ is a correction coefficient which will be detailed later, and $N_\Psi^{\rm stat}$ is the abundance from the statistical model. This assumes that all the c and $\bar{c}$ quarks are exclusively produced primordially, and populate open and hidden charm states according to relative chemical equilibrium. The equilibrium abundance of regenerated charmonia is given by

$$N_\Psi^{stat} = \gamma_c^2 V n_\Psi \quad (6)$$

with V: the volume of the fireball, n_Ψ: chemical equilibrium density of charmonium Ψ, and γ_c: charm quark fugacity. The latter is determined by the canonical charm conservation equation,

$$N_{c\bar{c}} = \frac{1}{2}\gamma_c V n_{op}\frac{I_1(\gamma_c V n_{op})}{I_0(\gamma_c V n_{op})} + \gamma_c^2 V n_{hid} \quad (7)$$

with $N_{c\bar{c}}$: total number charm quark pairs produced, n_{op}: density of all open charm states, n_{hid}: density of all hidden charm states. In the present work we use the charm quark cross section d$\sigma_{\bar{c}c}/$d$y(y=0)$=95 μb in line with recent PHENIX measurements [26] (with the assumption that 30% of the total produced charm are uniformly distributed over 1.8 rapidity units which is the rapidity coverage of our fireball). For the rapidity dependence we take guidance from perturbative QCD calculation [27], leading

to $\mathrm{d}\sigma_{c\bar{c}}/\mathrm{d}y(y{=}1.7){=}60$ μb. Currently the uncertainties of charm production in both theoretical predictions and experimental measurements are rather large. The modified Bessel function factor $\frac{I_1(\gamma_c V n_{op})}{I_0(\gamma_c V n_{op})}$ on the r.h.s accounts for exact $c\bar{c}$ conservation in the canonical ensemble relative to grand-canonical ensemble [28,29].

The abundance of charmonia, N_Ψ^{stat}, from the statistical model is subject to two additional corrections to obtain N_Ψ^{eq} in the rate equation Eq.(2). The first correction simulates incomplete charm quark thermalization in medium: It is natural to expect that the coalescence rate from non-thermalized c and $\bar{c}$ quarks is smaller than for fully thermalized charm quarks [30,31]. We implement this correction by multiplying the charmonium abundances from the statistical model in a schematic way by a factor $\mathcal{R} = 1-\exp(-\tau/\tau_{eq}^c)$, where τ_{eq}^c is the thermal relaxation time of charm quarks which is the second main parameter in our approach. The second correction is a "correlation volume" V_{corr} for the coalescing charm quarks [5]. The correlation volume increases Ψ production because the $c\bar{c}$ pairs do not have time to populate the entire fireball volume. We implement this correction by replacing the fireball volume V in the argument of the Bessel function by a correlation volume V_{corr} in Eq.(7). The "correlation volume" is estimated as the volume explored by a receding $c\bar{c}$ pair: $V_0(\tau){=}4\pi(r_0+\langle v_c\rangle\tau)^3/3$, where $r_0{\simeq}1.2$ fm represents a minimal radius characterizing the range of strong interactions, and $\langle v_c\rangle$ denotes the average relative speed of the produced c and $\bar{c}$ quarks which we vary between $0.5c$ and $0.8c$. Within this setup we adjust our second parameter τ_{eq}^c to the inclusive J/ψ yield in central Au-Au at RHIC at midrapidity, resulting in τ_{eq}^c=4-7 fm/c, corresponding to $\langle v_c\rangle{=}0.8c$ and $0.5c$, respectively.

The transverse momentum distributions of regenerated charmonia are approximated by local thermal equilibrium and boosted by the transverse flow of the medium, corresponding to a blastwave expression [32],

$$\left.\frac{\mathrm{d}N_\Psi}{p_t\mathrm{d}p_t}\right|_{coal} \propto m_t \int_0^R r\mathrm{d}r K_1\left(\frac{m_t\cosh y_t}{T}\right) I_0\left(\frac{p_t\sinh y_t}{T}\right) \tag{8}$$

with $m_t{=}\sqrt{m_\Psi^2+p_t^2}$, transverse rapidity $y_t{=}\tanh^{-1}v_t(r)$ with linear flow profile $v_t(r){=}v_s\frac{r}{R}$ and surface velocity v_s given by the fireball evolution formula, Eq.(5). We evaluate the blastwave expression at the hadronization transition (T_c=180 MeV) and neglect rescattering of Ψ's in the hadronic phase.

4 Centrality and Rapidity Dependence

The number of J/ψ produced in initial hard collisions at given impact parameter (b) is estimated from the production cross section in p-p collisions and then scaled by number of binary collisions in N-N collisions, $N_{coll}(b)$. We use the J/ψ production cross section from PHENIX data [33] with $\mathrm{d}\sigma_{pp}^{J/\psi}/\mathrm{d}y{=}750(500)$ nb (with about 30% uncertainty) at mid (forward) rapidity. The centrality dependence of the inclusive J/ψ yield in terms of nuclear

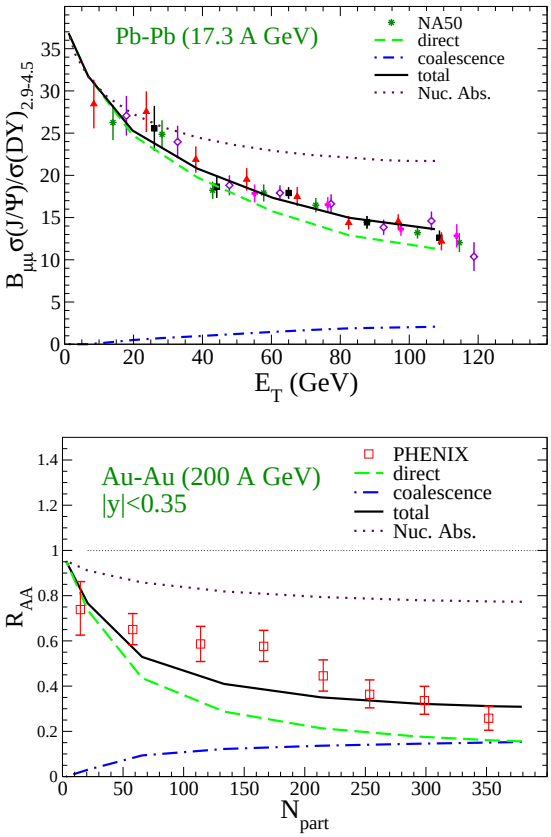

Fig. 2. (Color online) Results of the thermal rate-equation approach for $R_{AA}^{J/\psi}$ vs. centrality at SPS (upper panel) and RHIC midrapidity (lower panel) are compared to NA50 [2] and PHENIX data [3]. Solid line: total J/ψ yield; dashed line: suppressed primordial production; dot-dashed line: regeneration component; dotted line: primordial production with nuclear absorption only.

modification factor,

$$R_{AA} = \frac{N_{J/\psi}^{AA}}{N_{J/\psi}^{pp}N_{coll}}\ , \tag{9}$$

is displayed in Fig. 2. For central collisions the direct and regeneration component are about equal (quite similar to Ref. [31]), while for peripheral collisions the direct component dominates because the lifetime of the medium is shorter so that there is less time for regeneration processes and for charm quarks to thermally equilibrate (reducing coalescence into charmonia). Fig. 2 also includes the strength of suppression caused by CNM effects (dotted line) and by the hot medium indicating the latter to be substantially larger than the former.

Next we proceed to the inclusive J/ψ yield at forward rapidity as shown in Fig. 3 with scenarios 1 and 2 for CNM effects. In scenario 1, where the CNM induced suppression at forward rapidity is assumed to be the same as at midrapidity, the hot medium causes slightly less suppression than at mid-rapidity due to a shorter QGP lifetime (recall Fig. 1). Concerning the regeneration component, we note that the number of charm quark pairs at RHIC energy is

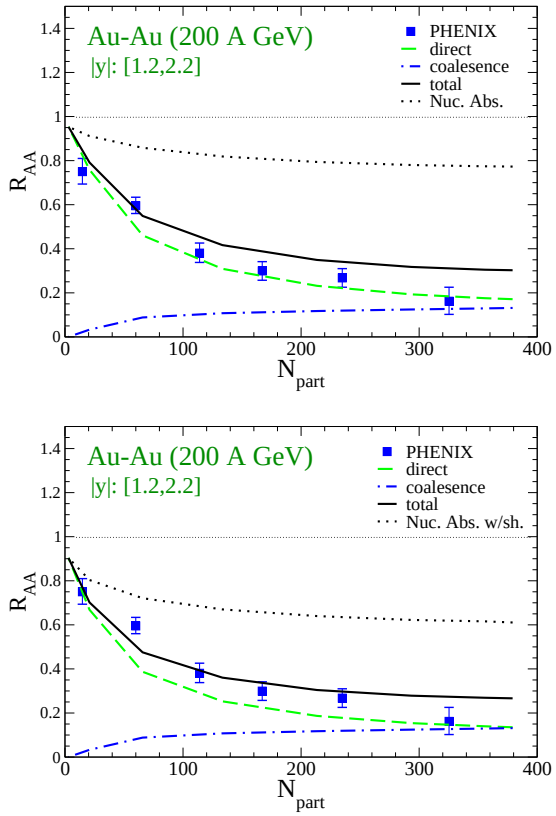

Fig. 3. (Color online) Results of the thermal rate-equation approach for $R_{AA}^{J/\psi}$ vs. centrality at forward rapidity compared to PHENIX data [3] with CNM effects in scenario 1 (upper panel) and scenario 2 (lower panel). Solid line: total J/ψ yield; dashed line: suppressed primordial production; dot-dashed line: regeneration component; dotted line: primordial production with CNM effects only.

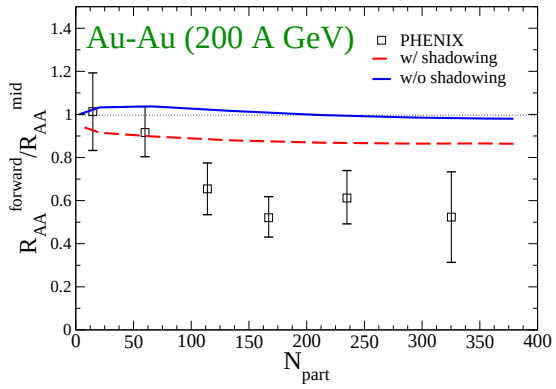

Fig. 4. (Color online) The thermal rate-equation approach results of ratio of forward and midrapidity J/ψ R_{AA} versus N_{part} with cold nuclear matter effects in scenario 1 (solid line) and scenario 2 (dashed line) compared to PHENIX data [3].

between the canonical and grandcanonical limit, so that $N_{\Psi}^{stat} \sim N_{c\bar{c}}^{\alpha}$ with α between 1 (canonical limit) and 2 (grandcanonical limit) as following from the charm conservation equation (7). If charm and J/ψ production in p-p collisions (the denominator in R_{AA}) are less at forward rapidity than at midrapidity by about the same fraction, the reduction of regeneration component at forward rapidity is about $R_{AA} \sim N_{c\bar{c}}^{\alpha-1}$. Adding up the two components the total J/ψ yield at forward rapidity is almost equal to that at midrapidity since the slight decrease in the regeneration component is compensated by the slight increase in the direct component, see upper panel of Fig. 3. Scenario 2 differs from scenario 1 in that the direct component at forward rapidity is subject to stronger CNM suppression. Consequently, the inclusive J/ψ yield at forward rapidity is more suppressed which leads to better agreement with experimental data as seen in the lower panel of Fig. 3. To better illustrate the comparison between forward and midrapidity we plot the ratio of forward and midrapidity J/ψ R_{AA} and compare to experimental data in Fig. 4. Even with a stronger cold matter induced suppression at forward rapidity due to shadowing (scenario 2) our approach still appears not to fully account for the experimental findings. However one needs to keep in mind that the current uncertainties in several key inputs, in particular charm production cross section at forward rapidity and shadowing, are still appreciable. More accurate *d-Au* data will enable more definite conclusions.

Finally we calculate the $\chi_c/(J/\psi)$ and $\psi'/(J/\psi)$ ratios which may provide additional discrimination of charmo-

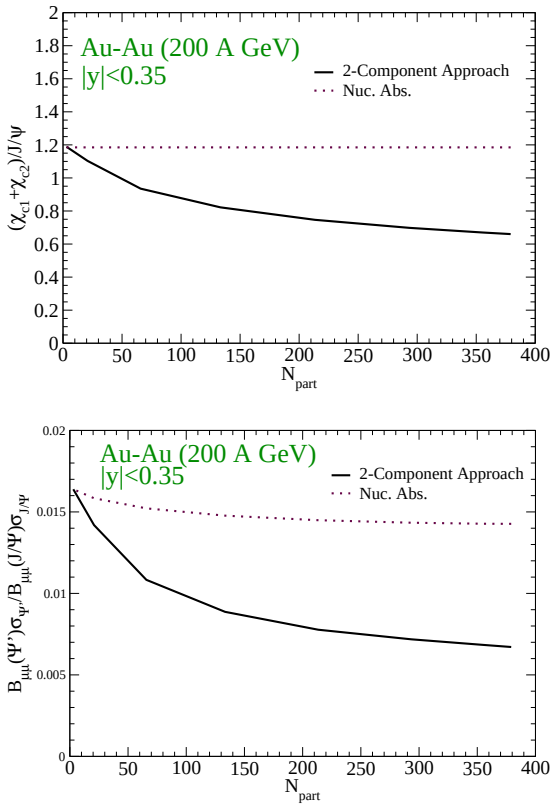

Fig. 5. (Color online) Results of the thermal rate-equation approach for the $(\chi_{c1}+\chi_{c2})/(J/\psi)$ ratio (upper panel) and $\psi'/(J/\psi)$ ratio (lower panel) vs. centrality at midrapidity at RHIC. Solid line: the results of the thermal rate-equation approach; dashed line: the nuclear absorption only. The J/ψ's in the denominator include feeddown from χ_c and ψ'.

nium production mechanisms: *e.g.*, the gluo-dissociation process and quasifree dissociation process give comparable suppression for J/ψ but for χ_c the gluo-dissociation process gives much larger dissociation rate [6] leading to a much smaller $\chi_c/(J/\psi)$ ratio. As another example, if formation time effects [20,34,35] are important one may observe less suppression of χ_c than J/ψ due to a longer [35] formation time of χ_c compared to J/ψ, together with a smaller dissociation cross section for a "pre-hadronic" $c\bar{c}$ pair than for a fully formed charmonium. This is in contrast to most standard dissociation mechanisms (since χ_c is a higher excited $c\bar{c}$ state than J/ψ with smaller binding energy and therefore is more easily destroyed) and regeneration mechanism (χ_c is heavier so that its equilibrium abundance is suppressed compared to J/ψ by the Boltzmann thermal factor).

For χ_c states, we constrain ourselves to χ_{c1} and χ_{c2} with a combined average branching ratio of 27% into J/ψ's [36]. The resulting $\chi_c/(J/\psi)$ and $\psi'/(J/\psi)$ ratio at midrapidity are shown in Fig. 5. Both drop with centrality below the ratios obtained from CNM-induced suppression (we assume that J/ψ and χ_c undergo the same strength of CNM-induced suppression).

5 Transverse Momentum Spectra

In order to gain further insights into charmonium production mechanisms, and to discriminate among them, we investigate the transverse momentum spectra of J/ψ. Let us again start at midrapidity: The centrality dependence of $\langle p_t^2\rangle$ is shown in the upper panel of Fig. 6. The $\langle p_t^2\rangle$ for the direct component increases with centrality due to a stronger Cronin effect generated by a longer path length $\langle l\rangle$ travelled by the gluon pair (recall Section 2) in more central collisions. The $\langle p_t^2\rangle$ of the regeneration component also increases with centrality due to an increase of the radial flow velocity at the end of mixed phase. However, the magnitude of $\langle p_t^2\rangle$ of the regeneration component is much smaller than primordial production at all centralities. The main point is that for more central collisions the regeneration component makes up an increasing fraction of the total yield leading to an almost constant $\langle p_t^2\rangle$ with centrality, consistent with current PHENIX data. Similar results are also obtained by the kinetic recombination model of Ref. [8]. On the contrary, at SPS energy, the direct component dominates at all centrality so that the Cronin effect dominates leading to a monotonically increasing $\langle p_t^2\rangle$, see lower panel of Fig. 6. A decreasing $\langle p_t^2\rangle$ with centrality is thus a supporting signature of the presence of regeneration. More definite conclusions will be possible with improved data accuracy.

We now turn to the $\langle p_t^2\rangle$ vs. centrality at forward rapidity as shown in Fig. 7 (with CNM effects in scenario 1). Within the current uncertainties in the Cronin effect our results agree with experimental data. The increase of $\langle p_t^2\rangle$ suggests that the direct component at forward rapidity is substantial; otherwise the $\langle p_t^2\rangle$ would be significantly smaller.

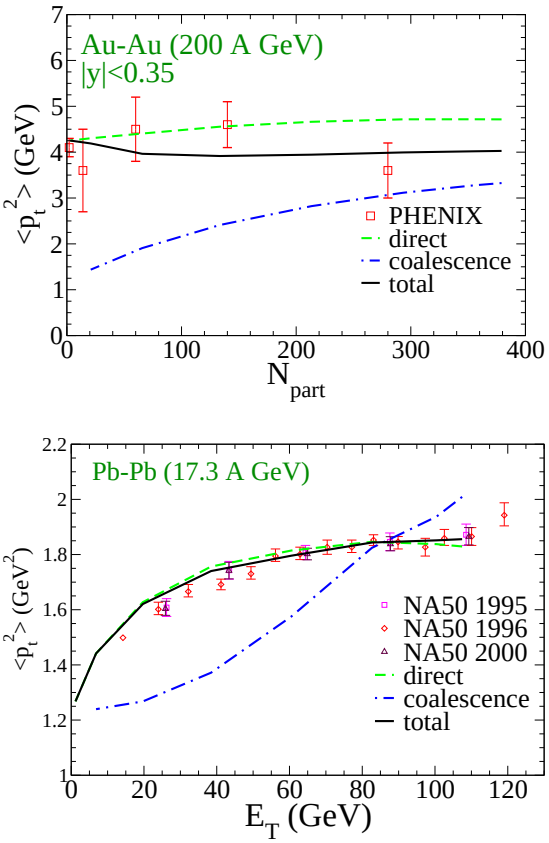

Fig. 6. (Color online) Results of the thermal rate-equation approach for $\langle p_t^2\rangle$ vs. centrality at RHIC midrapidity (upper panel) and SPS (lower panel) compared to PHENIX [3] and NA50 data [37,15]. Solid line: $\langle p_t^2\rangle$ for the total J/ψ yield (direct component + regeneration component); dashed line: $\langle p_t^2\rangle$ for the direct component; dot-dashed line: $\langle p_t^2\rangle$ for the regeneration component.

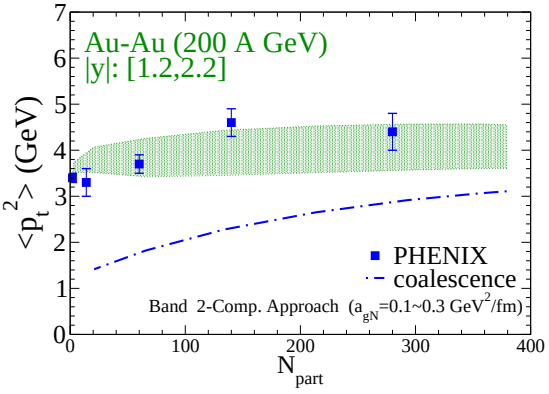

Fig. 7. (Color online) Results of the thermal rate-equation approach for $\langle p_t^2\rangle$ vs. centrality at forward rapidity compared to PHENIX data [3]. The band represents the $\langle p_t^2\rangle$ for the total J/ψ yield (direct + regeneration). The width of the band represents the uncertainty from the strength of the Cronin effect (estimated from *d-Au* data with a_{gN}=0.1-0.3 GeV^2/fm). The cold nuclear matter effects are implemented in scenario 1. Dot-dashed line: $\langle p_t^2\rangle$ for the regeneration component.

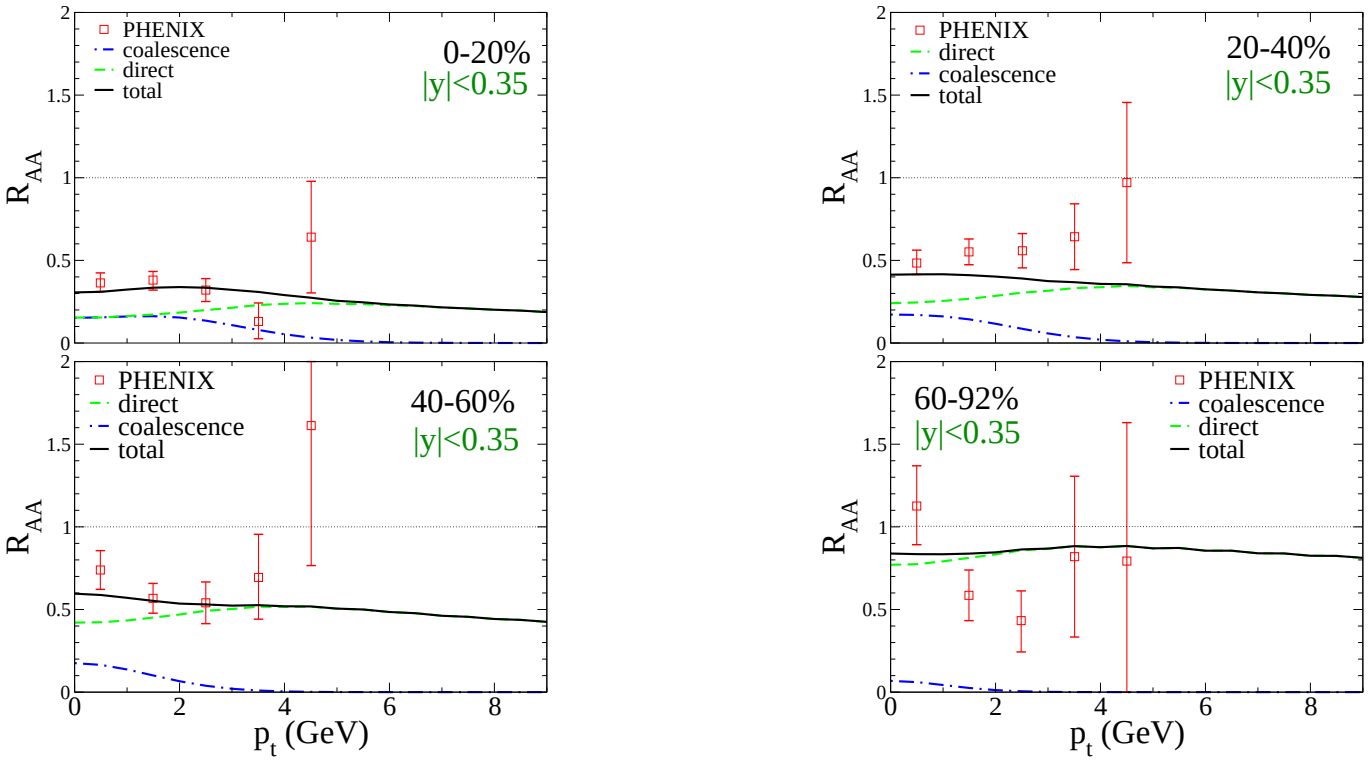

Fig. 8. (Color online) Results of the thermal rate-equation approach for $R_{AA}^{J/\psi}$ vs. transverse momentum for different centrality selections at midrapidity are compared to PHENIX data [3]. Solid line: total J/ψ yield; dashed line: suppressed primordial production; dot-dashed line: regeneration component. The Cronin effects are implemented with a_{gN}=0.1 GeV^2/fm.

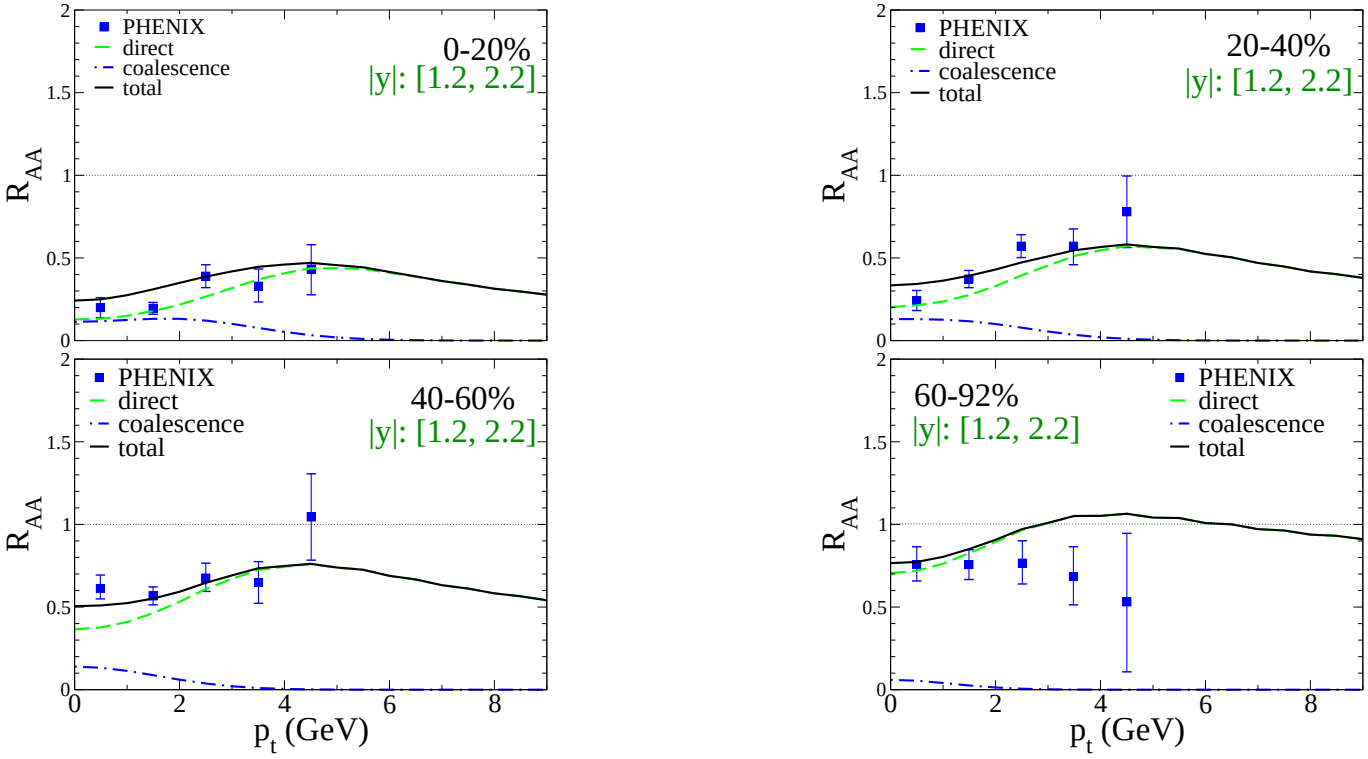

Fig. 9. (Color online) Results of the thermal rate-equation approach for $R_{AA}^{J/\psi}$ vs. transverse momentum for different centrality selections at forward rapidity are compared to PHENIX data [3]. Solid line: total J/ψ yield; dashed line: suppressed primordial production; dot-dashed line: regeneration component. The CNM effects are implemented in scenario 1 with a_{gN}=0.2 GeV^2/fm.

For a more differential comparison with experimental data we plot $R_{AA}(p_t)$ for different centrality selections at both mid- and forward rapidity (with CNM effects in scenario 1 and a_{gN}=0.2 GeV^2/fm) in Fig. 8 and 9 respectively. Overall, our model results reproduce $R_{AA}(p_t)$ data reasonably well. By comparing forward and midrapidity results there is an indication for stronger suppression at forward rapidity relative to midrapidity mainly in the low p_t regime (for central and semicentral collisions). Less regeneration and stronger Cronin effect at forward rapidity can both generate such an effect.

6 Conclusion

In this work we have applied a previously constructed thermal rate-equation approach to study charmonium production in 200 AGeV *Au-Au* collisions at RHIC at forward rapidity and compared to midrapidity results. Our calculations reasonably reproduce the experimental data of inclusive J/ψ R_{AA}, $\langle p_t^2 \rangle$ and p_t spectra at forward rapidity. We find that the observed stronger suppression at forward rapidity can be partially attributed to smaller regeneration resulting from smaller open charm production but additional suppression from cold nuclear matter effects (shadowing) is required as well. An accurate knowledge of shadowing will be needed to clarify the "puzzle" of the stronger suppression at forward rapidity. As a next step we will improve our current treatment of the coalescence of c and $\bar{c}$ quarks by performing a microscopic calculation with a time-dependent charm quark distribution based on Ref. [38], which will allow for a more accurate evaluation of regeneration effects, especially their dependence on incomplete charm-quark equilibration. We also look forward to new experimental data to better constrain the inputs of our approach which will pave the way for more quantitative conclusions.

References

1. T. Matsui and H. Satz, Phys. Lett. B **178** (1986) 416.
2. L. Ramello *et al.* [NA50 Collaboration], Nucl. Phys. A **715** (2003) 243.
3. A. Adare *et al.* [PHENIX Collaboration], Phys. Rev. Lett. **98** (2007) 232301.
4. P. Braun-Munzinger and J. Stachel, Nucl. Phys. A **690** (2001) 119
5. L. Grandchamp, R. Rapp and G. E. Brown, Phys. Rev. Lett. **92** (2004) 212301.
6. X. Zhao and R. Rapp, Phys. Lett. B **664** (2008) 253
7. L. Grandchamp and R. Rapp, Phys. Lett. B **523** (2001) 60.
8. R. L. Thews and M. L. Mangano, Phys. Rev. C **73**, 014904 (2006)
9. M. E. Peskin, Nucl. Phys. B **156** (1979) 365; G. Bhanot and M. E. Peskin, Nucl. Phys. B **156** (1979) 391.
10. A. Andronic, P. Braun-Munzinger, K. Redlich and J. Stachel, Nucl. Phys. A **789** (2007) 334.
11. N. Armesto and A. Capella, Phys. Lett. B **430** (1998) 23
12. A. Capella, L. Bravina, E. G. Ferreiro, A. B. Kaidalov, K. Tywoniuk and E. Zabrodin, arXiv:0712.4331 [hep-ph].
13. C. W. De Jager, H. De Vries and C. De Vries, Atom. Data Nucl. Data Tabl. **14** (1974) 479.
14. A. Adare *et al.* [PHENIX Collaboration], Phys. Rev. C **77** (2008) 024912
15. N. S. Topilskaya *et al.* [NA50 Collaboration], Nucl. Phys. A **715** (2003) 675.
16. X. Zhao and R. Rapp, arXiv:0806.1239 [nucl-th].
17. M. Asakawa and T. Hatsuda, Phys. Rev. Lett. **92** (2004) 012001
18. D. Cabrera and R. Rapp, Phys. Rev. D **76** (2007) 114506
19. F. Karsch, R. Petronzio, Phys. Lett. B **193** (1987) 105.
20. J.P. Blaizot, J.Y. Ollitrault, Phys. Rev. D **39** (1989) 232.
21. J. Huefner and P. f. Zhuang, Phys. Lett. B **559** (2003) 193
22. I. Arsene *et al.* [BRAHMS Collaboration], Nucl. Phys. A **757** (2005) 1
23. B. B. Back *et al.*, Nucl. Phys. A **757** (2005) 28
24. K. Adcox *et al.* [PHENIX Collaboration], Nucl. Phys. A **757** (2005) 184
25. M. Cheng *et al.*, Phys. Rev. D **74** (2006) 054507
26. A. Adare *et al.* [PHENIX Collaboration], Phys. Rev. Lett. **97** (2006) 252002
27. M. Cacciari, P. Nason and R. Vogt, Phys. Rev. Lett. **95** (2005) 122001
28. J. Cleymans, K. Redlich and E. Suhonen, Z. Phys. C **51** (1991) 137.
29. M. I. Gorenstein, A. P. Kostyuk, H. Stoecker and W. Greiner, Phys. Lett. B **509** (2001) 277
30. V. Greco, C. M. Ko and R. Rapp, Phys. Lett. B **595** (2004) 202
31. L. Yan, P. Zhuang and N. Xu, Phys. Rev. Lett. **97** (2006) 232301
32. E. Schnedermann, J. Sollfrank and U. W. Heinz, Phys. Rev. C **48** (1993) 2462.
33. A. Adare *et al.* [PHENIX Collaboration], Phys. Rev. Lett. **98** (2007) 232002.
34. S. Gavin, R. Vogt, Nucl. Phys. B **345** (1990) 104.
35. F. Karsch, R. Petronzio, Z. Phys. C **37** (1988) 627.
36. W. M. Yao *et al.* [Particle Data Group], J. Phys. G **33** (2006) 1.
37. M. C. Abreu *et al.* [NA50 Collaboration], Phys. Lett. B **499** (2001) 85.
38. H. van Hees, M. Mannarelli, V. Greco and R. Rapp, Phys. Rev. Lett. **100** (2008) 192301